



## **MICROTREMOR ARRAY MEASUREMENTS FOR SITE EFFECT INVESTIGATIONS: COMPARISON OF ANALYSIS METHODS FOR FIELD DATA CROSSCHECKED BY SIMULATED WAVEFIELDS**

**Matthias OHRNBERGER<sup>1</sup>, Estelle SCHISSELE<sup>2</sup>, Cecile CORNOU<sup>3</sup>, Marc WATHELET<sup>4</sup>,  
Alexandros SAVVAIDIS<sup>5</sup>, Frank SCHERBAUM<sup>6</sup>, Denis JONGMANS<sup>7</sup>, Fortunat KIND<sup>8</sup>**

### **SUMMARY**

Within the scope of the SESAME project we have assessed the reliability of array techniques applied to ambient vibrations for site effect investigation. In particular, we estimated the dispersion characteristics for the Rayleigh wave part of ambient vibrations recorded in the Lower Rhine Embayment (NW Germany). In order to eliminate ambiguities related to the interpretation of the estimated phase velocities, we crosschecked our results with simulated microtremor wavefields. The inversion of the observed dispersion curves shows that there is a good agreement with the known shear wave velocity profiles of the subsurface.

### **INTRODUCTION**

The quantitative assessment of site effects, that is the ground motion effects associated with the local surface geology (e.g. Borchardt [1]), is a major issue in seismic hazard and engineering seismology studies. Frequency dependent site amplifications are known to be mainly caused by reverberations and resonance effects of S-waves within unconsolidated sediments overlaying stiffer formations. Thus, it is of key interest to determine the shallow shear wave velocity structure (Hartzell et al. [2], Yamanaka [3]). In recent years, the passive recording of microtremors at single stations (e.g. Bard [4], Ishida et al. [5], Fäh et al. [6],[7], Arai and Tokimatsu [8]) or at small-scale arrays (e.g. Horike [9], Matsushima and Okada [10], Tokimatsu et al. [11], Tokimatsu [12], Scherbaum et al. [13]) has gained considerable attention for the determination of shallow shear wave velocity profiles. The major advantages of these ambient vibration techniques are the low cost exploration and monitoring capabilities, the possibility to perform non-destructive measurements at every place of a densely populated city, and the relatively large penetration depth.

---

<sup>1</sup>Institute of Geosciences, University of Potsdam, Potsdam, Germany

<sup>2</sup>Institute of Geosciences, University of Potsdam, Potsdam, Germany

<sup>3</sup>Schweizer Erdbebendienst, SED, ETHZ, Switzerland

<sup>4</sup>GEOMAC, Université of Liege, Belgium

<sup>5</sup>Institute of Engineering Seismology & Earthquake Engineering (ITSAK), Thessaloniki, Greece

<sup>6</sup>Institute of Geosciences, University of Potsdam, Potsdam, Germany

<sup>7</sup>LIRIGM, Université Joseph Fourier, Grenoble, France.

<sup>8</sup>Schweizer Erdbebendienst, SED, ETHZ, Switzerland

However, one of the main difficulties of microtremor array analysis methods for the determination of shear wave velocity profiles consists in the reliable identification and interpretation of the dispersion characteristics of the surface wave part contained in the ambient noise wavefield. Furthermore, in case of complex ambient vibration wavefield situations, it is difficult to assess whether the underlying assumptions of commonly employed array techniques are fulfilled and to validate the reliability of measured phase velocities. It is evident that a biased estimate of phase velocities or an inadequate interpretation of dispersion curve branches has considerable consequences for the inverted shear wave velocity structures (Forbriger [14]). The accuracy of shear wave velocity models derived from ambient vibration array methods is therefore still debated (e.g. Wills [15], Boore and Brown [16], Ohrnberger et al. [17]).

Within the scope of the ongoing EU-project SESAME (Site *E*ffect*S* assessment using *A*Mbient *E*xcitation, EU-Grant EVG1-CT-2000-00026) (Bard [18]), both practical and theoretical aspects of single station H/V analysis as well as microtremor array analysis methods are evaluated (Atakan et al. [19], Duval et al. [20], Bonnefoy-Claudet et al. [21], Cornou et al. [22], Ohrnberger et al. [23]) with the final aim to provide practical guidelines for the application of these techniques for site effect studies (Koller et al. [24]).

In this study we focus on the reliable determination of Rayleigh wave dispersion curves from ambient vibration array recordings. In particular we processed microtremor data measured at a specific site in the Lower Rhine Embayment (NW Germany) with different array methods. We chose this location as the subsurface structure of this region is relatively well known and preceding work has been accomplished for this site (Budny [25], Ibs von Seht and Wohlenberg [26], Parolai et al. [27], Hinzen et al. [28], Scherbaum et al. [13], Ohrnberger et al. [17]). This allowed us to simulate surface wave ambient vibration wavefields for a general reference velocity model using simplified assumptions about the type of source excitation and spatial distribution. The aim of the wavefield modeling is to support the interpretation of the observed dispersion characteristics for the real wavefield situation.

## MEASUREMENT SITE AND FIELD DATA

The city of Cologne, with a population close to 1 million, is located near the southeastern end of the Lower Rhine Embayment (LRE) in NW Germany, which is one of the most active seismic regions in Central Europe (Fig. 1). The shallow subsurface structure consists of soft Quaternary and Tertiary sediments overlaying Devonian shales and sandstones, which outcrop to the northeast and southwest.

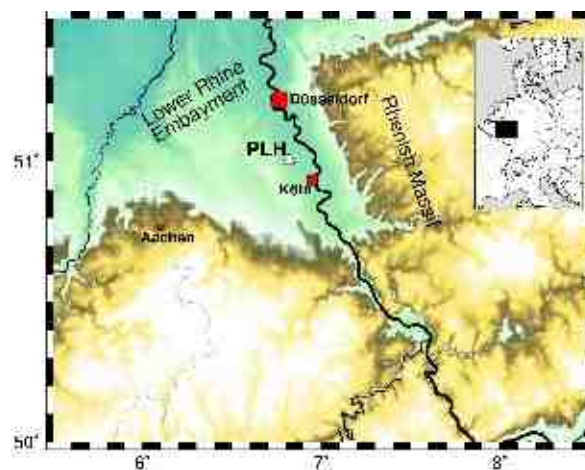


**Fig. 1: Measurement site at Pulheim (PLH) in the Lower Rhine Embayment (NW Germany)**

For a site in the vicinity of the city, an ambient vibration array experiment was performed near Pulheim (PLH, Fig. 1). The array (aperture  $\sim 1$  km) consisted of 12 elements, which were equipped with Lennartz LE5D three-component seismometers with an eigenperiod of 5 s. Owing to access constraints, the arrays were operated as cross arrays following local dirt roads and/or small trails (Fig. 2). Several hours of ambient vibrations were recorded using a sampling frequency of 125 Hz. The resolution capabilities of this configuration when using a conventional frequency wavenumber approach are depicted for two narrow frequency bands in Fig. 2.

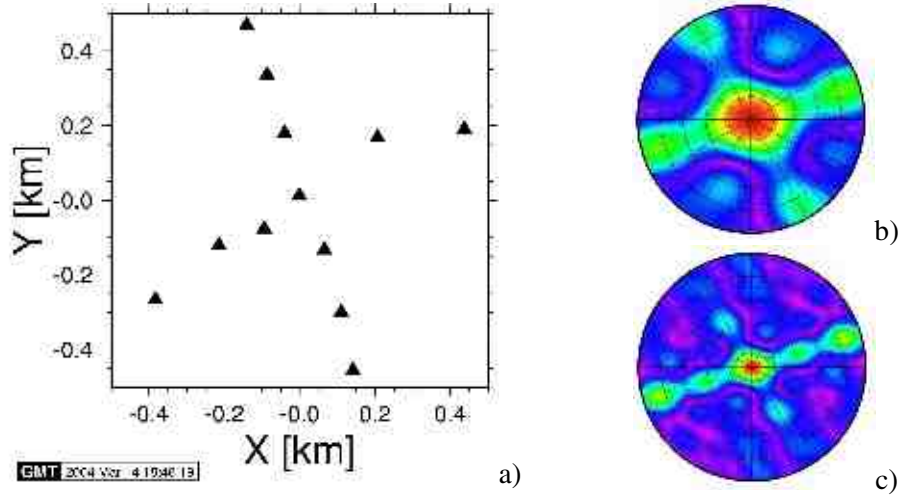


**Fig. 2: a) Station configuration of the array deployment used in Pulheim. The aperture is approx. 900 m and the average interstation distance is in the order of 150 m. Right panel: Array response functions for the station distribution for the narrow frequency bands b) 0.45 to 0.55 Hz and c) 0.9 to 1.1 Hz.**

For the LRE, several ambient noise studies (Ibs von Seht and Wohlenberg [26], Parolai et al. [27], Hinzen et al. [28]) have been performed providing shear wave velocity depth models for the region using single station H/V ratios. Scherbaum et al. [13] obtained shear wave velocity profiles from a combined inversion of dispersion curves and H/V ratios derived from ambient vibration recordings for the site Pulheim (PLH). From the analysis of local earthquake records slight modifications of this model have been suggested by Ohrnberger et al. [17].

Following the classification within the new German earthquake code, the situation in the LRE is well described by the deep basin model (subsoil class C, DIN 4149new, Brüstle and Stange [29], Brüstle et al. [30]). This deep basin model is characterized by a shallow (20 m) soil layer with constant geotechnical parameters. This is followed by a subsoil soft sedimentary unit with increasing shear wave velocities from  $350 \text{ ms}^{-1}$  at 20 m down to  $800 \text{ ms}^{-1}$  at a depth of 320 m where the shear velocity is assumed to jump to  $1600 \text{ ms}^{-1}$ , which is representative of consolidated Permo-Mesozoic sediments. Below this depth, S-wave velocities are assumed to increase further with depth down to a reference bedrock depth of 1 km. Here a first-order velocity discontinuity is assumed. The half-space velocity is  $3300 \text{ ms}^{-1}$ .

## SIMULATION OF AMBIENT VIBRATION WAVEFIELD

In order to assess the interpretation of the results that we obtained from the processing of the data set recorded in Pulheim, we simulated ambient vibration wavefields for the same geologic situation that the one in the Lower Rhine Embayment. For P- and S- wave velocity models, we chose the generic deep basin model (Brüstle and Stange [29], Brüstle et al. [30]) of the new German earthquake code and adjusted this model slightly according to the study of Scherbaum et al. [13] to better resemble the real situation at site PLH. In particular we modified the depth of the main impedance contrast between

sedimentary layers and bedrock to a value of 210 m. The attenuation structure used for modeling have been taken from the work of Budny [25], who derived empirical models from downhole measurements in the LRE. Both the shear wave velocity depth function and  $Q_s$  attenuation structure used for the waveform modeling are shown in Fig. 3.

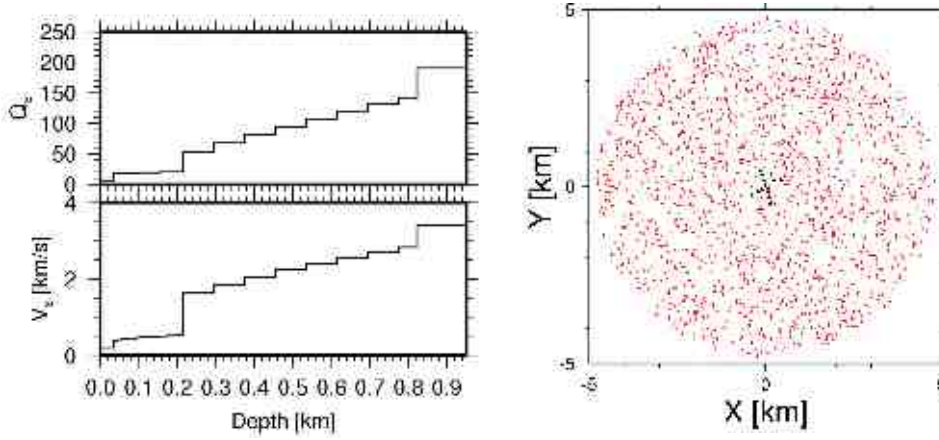


**Fig. 3: Left panel: shear wave velocity depth function and attenuation structure used for the waveform modeling for the Lower Rhine Embayment. Right panel: spatial distributions of the sources used for the waveform modeling (red dots). The black triangles represent the location of the different sensors of the array.**

Lacking a priori information of the spatial distribution and types of ambient vibration noise sources, we made simplified assumptions. In particular we used point-source excitations at the earth's surface with impulsive source time functions throughout this study. We used then the modal summation technique (Hermann [31]) in order to realize our simulation of ambient vibration wavefields. We considered randomly distributed sources on the medium surface (see Fig. 3) which are characterized by an equal density distribution in space with distances from the array center ranging from 0 to 5 km. Each source is repeated several times, and the number of repetition is chosen randomly between 1 and 5 (3 in average) (for details see Table 1). The time of excitation, the amplitude and the force orientations that characterize each source were also randomly chosen. The ambient vibration wavefields have been simulated for an array of 12 sensors resembling the geometrical configuration used for the Pulheim experiment (see Fig. 2).

Source configuration	Number of source locations	Number of excitations	Sources-array distances(km)	Modal summation seismograms
Random	2000	6000	0-5	32768 pts @ 50 Hz

**Table 1: Characteristics of the source configuration**

## ARRAY ANALYSIS RESULTS: REAL DATA VERSUS SIMULATIONS

### Frequency wave-number methods

In Ohrnberger et al. [23], we compared the performance of several frequency wavenumber techniques for the estimation of dispersion curve characteristics from ambient vibration recordings. From this study, we have shown that for this purpose, the most suitable methods are the conventional frequency wavenumber

decomposition (CVFK, after Kvaerna and Ringdahl [32]) and the high-resolution approach (CAPON, after Capon [33]).

The CVFK estimates, in sliding time window manner and narrow frequency bands around some center frequency, the parameters of propagation (direction and slowness) of the most coherent plane wave arrival. A grid search over the wavenumber plane is performed (equidistantly sampled in slowness and azimuth, azimuth and slowness resolution set to 5 degrees and 0.025 s/km, respectively).

The CAPON method is a high-resolution method, based on the estimation of the cross spectral matrix by a block-averaging technique of the observed signal contributions at the array stations for a given target frequency. This f-k technique has been widely used in the context of microtremor analysis (Tokimatsu [12]), especially because it allows high resolving capabilities in case of mixed wavefield situations.

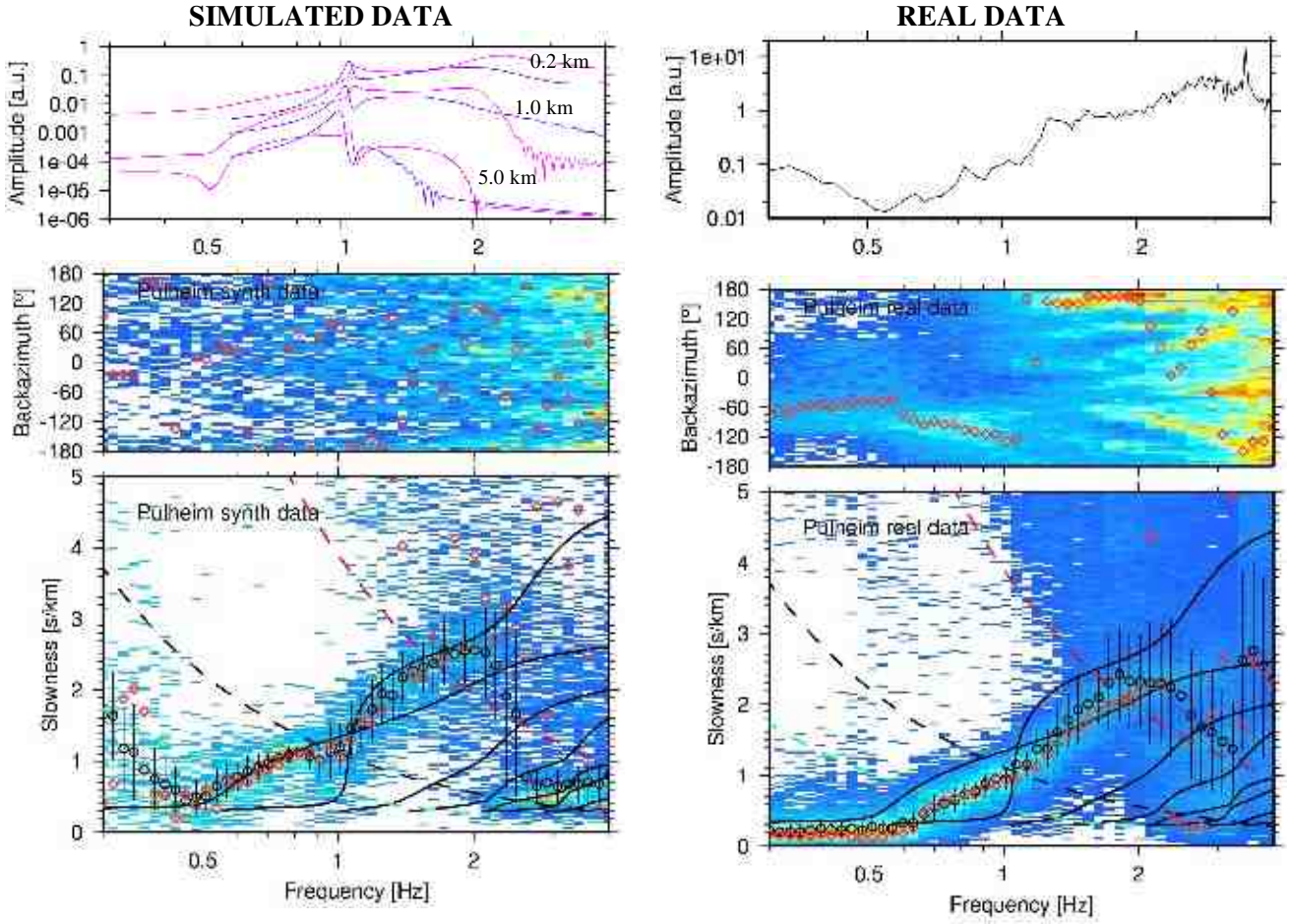
### The results

Fig. 4 shows both the slowness-frequency curves evaluated from the CVFK and CAPON analysis (lower panels) as well as the directional estimates (middle panels) for the simulated (left panels) and real (right panels) data sets. We choose to view the dispersion curves proportional to slowness instead of phase velocities, as this allows a linear relation to the measurement errors (time delays). Additional arguments for this way of displaying are given in Brown et al. [34]. The theoretical Rayleigh wave dispersion curves for fundamental and first higher modes are plotted for comparison (black curves). In addition, aliasing curves are plotted for the minimal (red dashed), mean (black dashed) and maximal (green dashed) interstation distance within the array configuration. We visualize the histograms obtained from the CVFK analysis as density plots, overlaid by the median and median deviation estimates. For the CAPON method, based on the block-averaged of the cross spectral matrix, we obtain a single slowness map per frequency for the whole analyzed time series. The upper left panel represents the spectral contribution for the fundamental and first higher modes calculated for three different distances of propagation (0.2, 1 and 5 km). The upper right panel represents the spectra of the observed data.

For the simulated data set, we observe that within the [0.6-1.9] Hz frequency band, both CVFK and CAPON follow the fundamental mode of dispersion curve. No stable estimates are observed in the frequency evolution of the direction of propagation, what reflects the random source configuration used for the simulation. However, around 1Hz, we observe a decrease of slowness values for both CVFK and CAPON estimates. We relate this observation to the contribution of higher modes around this frequency. This is confirmed by the spectral contribution of each mode plotted in Fig. 4.

As the sources are randomly distributed in space and time, it is difficult to determine whether there exists a dominant wavefield energy contribution from a certain distance range. Therefore, we computed the spectral contributions for the fundamental and first higher modes for three different distances of propagation (0.2, 1 and 5 km). All spectra show that the energy of the first higher mode is overtaking the energy of the fundamental around one 1Hz. Apparently this creates a mixed multimode wavefield situation that we are able to detect but not to resolve. For this simulated example, we consider that the valid frequency band of reasonable slowness values is restricted to the [0.6-1.9] Hz frequency band. For lower frequencies ( $< 0.6\text{Hz}$ ), we observe large scattering of the slowness values estimates that we attributed to low spectral energy level in the spectra. We think that these small deviations are associated with numerical noise in the forward calculation of the simulated wavefield which deteriorates the phase delay estimates below a certain amplitude level. For higher frequencies ( $>1.9\text{Hz}$ ), the array analysis is limited by aliasing features, due to insufficient spatial sampling. In the same frequency band, the slowness distribution obtained from the CVFK exhibit contributions from higher modes of surface waves.





**Fig. 4: Results of the CVFK (histograms overlaid by the median and median deviation estimates (black dots)) and the Capon (red dots) analysis for the simulated (lower left panel) and real (lower right panel) datasets. Lower panels: directional and slowness estimates, theoretical Rayleigh wave dispersion curves (black solid) and aliasing conditions (dashed lines). The upper left panel represents the spectral contribution of the fundamental and first higher modes (pink and violet respectively) for three different distances of propagation (0.2, 1 and 5km) and the upper right panel represents the spectra of the observed data.**

As for the simulated data set, we observe stable estimates of the slowness values within the [0.6 - 1.9] Hz frequency band for the real data set. From the source distribution we recognize a different situation than in the simulated case, since particularly stable direction of propagation are observed within this frequency band. Compared to the theoretical dispersion corresponding to the simulated wavefield, both CVFK and CAPON values exhibit slower slowness values. Nevertheless, the global shape of the observed dispersion curves is similar to what is expected. Interestingly, we do not observe any contribution of higher modes around 1Hz, as it was the case for the simulated data. For frequencies  $f < 0.6$  Hz, we still observe stable estimates of the slowness values. However, the spectral low at 0.55Hz (left uppermost panel) of the observed vertical component spectrum coincides with the H/V peak location (Scherbaum et al. [13]). Therefore, interpreting the H/V ratio from the Rayleigh wave ellipticity, we should not observe phase velocities of the fundamental mode Rayleigh wave around this frequency. We assume that for this frequency range either the array configuration shows too low resolution to separate wavefield contributions from different azimuths or the wavefield is composed of body waves traveling at higher (apparent) phase velocities. In any case, these values can be discarded from interpretation as the very high shear wave velocity for the bedrock (around 5km/s) are not realistic. Finally, for frequencies higher than

1.9Hz, the aliasing features are clearly visible, as for the simulated data set, but no clear contribution of higher modes are observed.

### Spatial autocorrelation method (SPAC) and modification

Whereas the frequency wavenumber techniques are based on the assumption of the validity of the plane wave signal model, the spatial autocorrelation method (SPAC, Aki [35]) bases its theoretical foundation on the precondition of a stochastic wavefield which is stationary in both time and space. Aki [35] showed, that, given this assumption, the existing relation between the spectrum densities in space and time can be used to derive the following expression:

$$\bar{\rho}(r, \omega) = J_0 \left( \frac{\omega r}{c(\omega)} \right) \quad \text{Eq. 1}$$

$\bar{\rho}(r, \omega) = \int_0^\pi \rho(r, \omega, \theta) d\theta$  represents the azimuthally averaged spatial autocorrelation  $\rho(r, \omega, \theta)$  for station pairs separated by distance  $r$  and the interstation direction  $\theta$ , and  $J_0$  denotes the Bessel function of the first kind and zero-th order. The above relation allows deriving the single valued phase velocity  $c(\omega)$  at a given frequency  $\omega$  by inversion from observed averaged spatial autocorrelation coefficients. Aki [35] suggested the use of dense semicircular array deployments to readily obtain these autocorrelation coefficients for various radii and target frequencies and applied this technique for the analysis of surface wave dispersion characteristics from microtremor recordings. Bettig et al. [36] suggested a modification of Aki's original SPAC formula which allows applying the spatial autocorrelation method for less ideal experimental array configurations. The modification concerns the evaluation of the averaged spatial autocorrelation coefficients from station pairs taken from rings of finite thickness instead of using a fixed radius. Practically, the values for minimal and maximal radii are determined from displaying the co-array configuration for arbitrary array geometries and selecting stations pairs with similar interstation distances and good azimuthal coverage for the computation of the averaged autocorrelation coefficients.

### The results

We have evaluated the spatial autocorrelation coefficients for the same datasets and station configuration as used for the f-k analysis by applying the MSPAC (modified SPAC) approach by Bettig et al. [36]. A direct comparison between the results obtained from the MSPAC method and the previously discussed f-k techniques involves the inversion of observed MSPAC curves into a dispersion curve. In order not to introduce additional ambiguities related to the stability of this non-linear inversion problem, we preferred to forward compute the theoretical autocorrelation curves from the theoretical dispersion curves.

In Fig. 5 we show the frequency dependence of the averaged spatial autocorrelation coefficients for the simulated and real data sets. From the co-array configuration we selected six rings with mean radii ranging from 150 m to 730 m. The number of station pairs in each ring varies from 7 to 16 and the azimuth range spanned ranges from 90 to nearly 180 degrees (except for the second ring which presents an azimuth coverage lower than 90 degrees). We additionally plotted the results of the CVFK and CAPON analysis results for these datasets. We converted the slowness-frequency pairs to frequency-spatial autocorrelation pairs for the minimal and maximal radius for each ring. The distribution of the CVFK results are shown as density plot, the CAPON results are given as individual point estimates.

## SIMULATED DATA

## REAL DATA

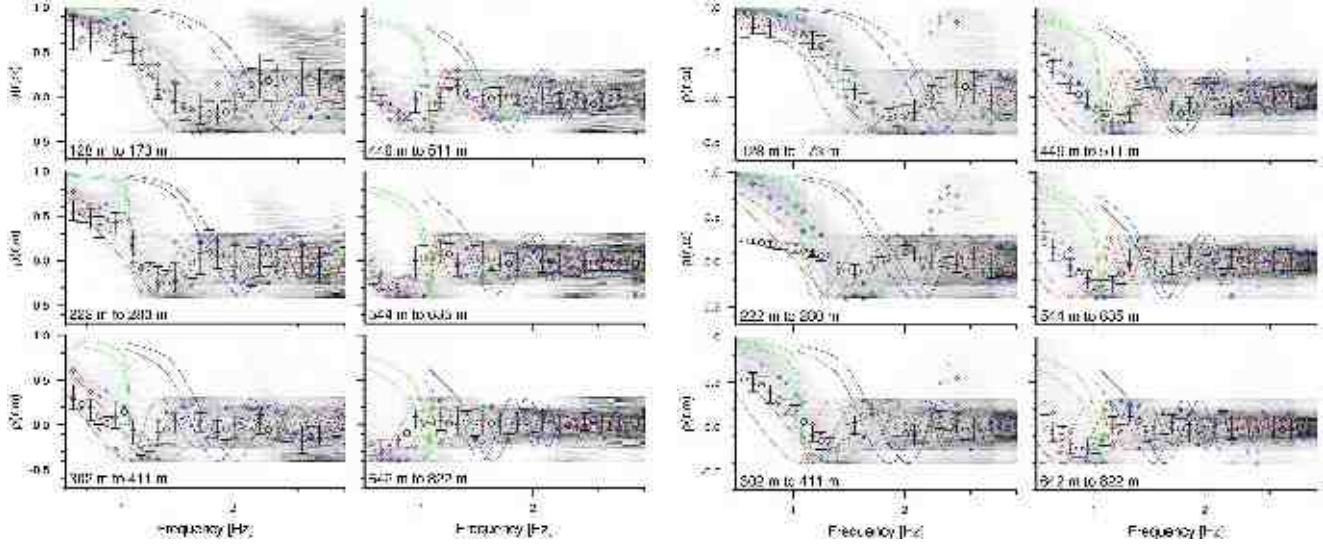


**Fig. 5: Averaged spatial autocorrelation coefficients evaluated for 50 frequencies between 0.7 Hz and 4.0 Hz (black dots). From top to bottom, the ring dimension increases from ca. 150 m to 730 m. The real and simulated are evaluated on the left and right panel respectively. Overlaid are the theoretical autocorrelation curves computed from the fundamental (red) and first two higher (green blue) modes for the given velocity model and for the minimum and maximum radii considered in each subplot. For the interpretation, see text.**

For the simulated data set, the comparison between the theoretical autocorrelation curves computed from the fundamental mode (red curve) of the Rayleigh wave dispersion curves and the observed correlation curves (black circles) are in good agreement, especially for the smaller rings. In addition, around 1Hz, we can clearly observe the contribution of the first higher mode. The auto-correlation curves show a clear deviation from the fundamental mode to the first higher (green curve) for various rings.

For the real data set, the observed autocorrelation curves apparently exhibit similar oscillation frequencies as the simulated ones. However, the curves appear to be shifted in frequency when compared to the theoretical curves. This observation is consistent with the results obtained from the frequency wavenumber decompositions where the observed dispersion show lower slowness values when compared to the synthetic model curves. As already pointed out by the f-k decomposition, we can find no indication of higher modes in the real data set.

For the second ring (222 to 280m), a mismatch of the observed auto-correlation coefficients is observed within the [0.7-1.2] Hz frequency band. The range of azimuth spanned by the co-array station pairs for this particular ring is less than  $90^\circ$  and as observed from the f-k analysis (Fig. 4), the wavefield presents a very stable direction of propagation for this frequency range. As a consequence the approximation of the averaged spatial autocorrelation coefficients by the Bessel function (Eq. 1) is no longer valid. This effect is also known as directional aliasing (Henstridge [37]). It should be noted, that this mismatch is not observed for the simulated data, as the spatial randomness of the source distribution compensates the small azimuthal coverage of station pairs.



## INTERPRETATION OF DISPERSION CURVES AND INVERSION RESULTS

Following the recommendations in Ohrnberger et al. [23] we compared three different analysis methods for both the simulated and experimentally obtained data sets. The comparison of the individual methods allow to derive a consistent interpretation of the dispersion characteristics in each case.

For the simulated data set we are able to detect the presence of higher mode contributions in the synthetic wavefield from an unexpected deviation of dispersion and spatial autocorrelation curves for a distinct frequency band (0.8-1.1 Hz). We can attribute this to the first higher mode, which energetically dominates the wavefield. However, this higher mode contribution can not be clearly separated nor can it be followed for a broader frequency range. Comparing the analysis results from different methods we determine the valid frequency band of dispersion curve interpretation to lie in the range between 0.6 and 1.9 Hz. Limitations are given from the occurrence of aliasing at higher frequencies and lack of energy for lower frequencies.

For the ambient vibration array recordings at PLH we are not able to detect any indication for the presence of higher mode surface waves contributing to the observed wavefield. However, a strong deviation of the stable slowness estimates from the fundamental mode predicted by the general reference model (Brüistle and Stange [29], Brüistle et al. [30]) is observed. Considering that the shear wave velocity profile for this model has been confirmed in previous studies (Scherbaum et al. [13]) this observation can not be easily explained. We speculated therefore whether the measured phase velocity curve could be better explained by higher mode contributions (e.g. first higher mode for frequencies above 1.3 Hz, Fig. 4 and Fig. 5). Nevertheless we reject this possible explanation for the following reason: considering the spectral contributions of individual mode branches for the simulated data set (relying on the reference model), the energetically dominance of the first higher mode should lie around 1 Hz and is relatively independent of the source – receiver geometry. In the analysis result we can not detect any remarkable behavior of the smoothly estimated dispersion curves at these frequencies. We conclude therefore, that we observe a dominating fundamental mode Rayleigh wave wavefield and the shift between the predicted and observed dispersion characteristics are due to discrepancies of the generic velocity model and the real site structure. As for the simulated analysis results, we set the valid frequency band for the interpretation of the dispersion characteristics to the range between 0.6 and 1.9 Hz. Limitations are given from the occurrence of aliasing at higher frequencies and inconsistently high phase velocities for the lower frequencies.

In order to provide high-quality dispersion curves for the inversion, we re-analyzed the data sets within the frequency band from 0.65 to 1.9 Hz (100 points logarithmically). We used the distributions of the 2% best values of the slowness maps derived for the high resolution CAPON approach to determine the median and median deviation of the frequency dependent slowness distributions as input data for the inversion procedure (compare Ohrnberger et al. [23]).

We used the inversion code implementation of Wathelet et al. [40] which employs the neighborhood algorithm (Sambridge [38],[39]) for inverting subsurface shear and compressional wave velocity profiles. The parametrization of the subsurface model was achieved by a two layer over halfspace model. The upper two layers represent here the sediment structure and are modeled as a stack of eight sublayers each with equal thickness following a power law velocity depth law. The free parameters of the inversion procedure are then for each sediment layer: the compressional and shear wave velocities of the uppermost sublayer of the stack, the power law exponent, the homogeneous density as well as the overall thickness of each sediment layer. Additionally, we inverted for the P and S-velocities and the density of the halfspace. The valid parameter ranges for the sampling of velocity models are given in Table 2.

Thickness [m]	Vp [m/s]	Vs [m/s]	$\rho$ [kg/cm <sup>3</sup> ]
[1,700]	[10,2000]	[1.,1414]	[1.9,2.3]
[1,700]	[500,5000]	[5,3535]	[2.0,2.6]
-	[500,7000]	[5,4950]	[2.0,2.6]

**Table 2: Allowed parameter range for the inversion procedure.**

The inversion results for the simulated data set are shown in Fig. 6. The best fitting dispersion curves and the respective corresponding velocity models are shown in blue colors. Interestingly, although the estimated dispersion characteristics (black dots with error bars) show a large scatter and mixed mode contributions in the frequency range 0.8 to 1.1 Hz, the synthetic shear wave velocity structure is well approximated for the shallow part until a depth of 200 m.

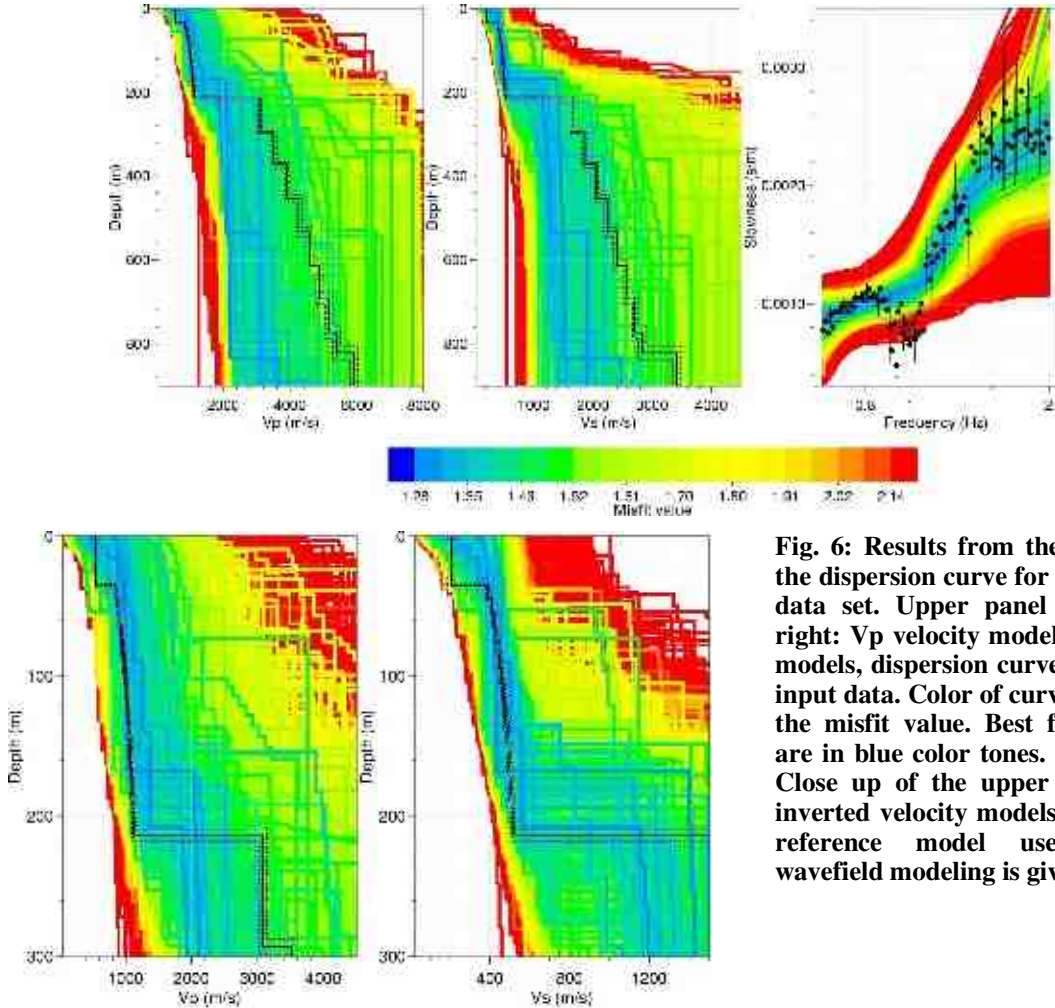


**Fig. 6: Results from the inversion of the dispersion curve for the simulated data set. Upper panel from left to right: Vp velocity models, Vs velocity models, dispersion curves overlaid by input data. Color of curves is given by the misfit value. Best fitting models are in blue color tones. Lower panel: Close up of the upper 300m of the inverted velocity models. The generic reference model used for the wavefield modeling is given in black.**

However, below the first strong impedance contrast, the structure can not be resolved. This can be explained by the restricted frequency band of the dispersion curve data. The shallowest part of the

reference model (above 35 m) can neither be obtained due the chosen parametrization in the inversion procedure.

The inversion results for the real data set at site PLH are shown in Fig. 7. Similar to the results obtained for the synthetic wavefield data set, the best ranked shear wave velocity profiles fit very well in the shallow part of the structure ( $<200\text{m}$ ) to both the generic reference model and the inversion results given by Scherbaum et al. [13]. On the other hand, the compressional wave velocity models showing a low misfit value tend to be in better agreement to the latter model. Scherbaum et al. [13], however, fixed the compressional wave velocity to a power law depth function provided by Budny [25] from downhole measurements for the LRE. This result indicates especially, that the compressional wave velocities have a significant influence on the resulting dispersion curves. We attribute the shift of the observed phase velocity curve compared to the forward calculated dispersion characteristics for the generic reference model to the change in compressional velocity rather than a difference in the shear velocity profile. Finally, the inverted deeper structures ( $>200\text{m}$ ) seem to resemble the generic reference model, but the range of models is too large to allow an interpretation of this part of the structure.

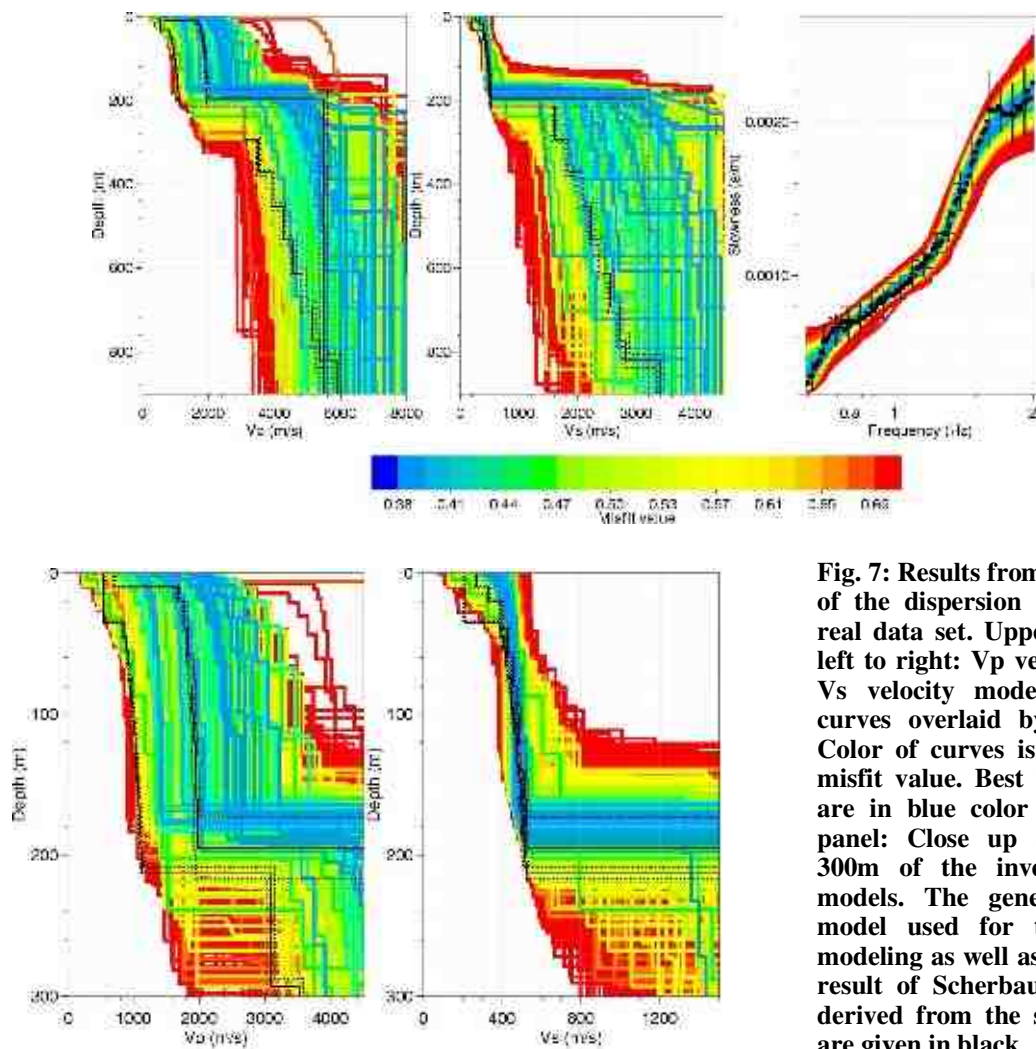


**Fig. 7: Results from the inversion of the dispersion curve for the real data set. Upper panel from left to right:  $V_p$  velocity models,  $V_s$  velocity models, dispersion curves overlaid by input data. Color of curves is given by the misfit value. Best fitting models are in blue color tones. Lower panel: Close up of the upper 300m of the inverted velocity models. The generic reference model used for the wavefield modeling as well as the inversion result of Scherbaum et al. [13] derived from the same data set are given in black**

## CONCLUSION

We have analyzed ambient vibration array recordings from a deep sediment site in NW Germany and compared the analysis results with those obtained for a simulated wavefield situation for this region. We have used this procedure as ambient noise excitation as well as particular propagation effects may lead to misinterpretation of phase velocities or autocorrelation coefficients obtained from array analysis. The use of various combinations of analysis methods may allow to prevent this eventual misinterpretation by providing complementary information on the ambient vibration wavefield characteristics. Contradictory results obtained from the individual methods may be an indicator to recognize such situations (see also Ohrnberger et al. [23]).

The combined use of analysis method applied to the wavefield simulations allowed us to interpret the real data with more confidence. We concluded for the real data set that the wavefield is dominated by fundamental Rayleigh waves and no higher mode wavefield contributions are observed in the usable frequency range for the inversion between 0.65 and 1.9 Hz. Furthermore, both the f-k techniques as well as the strong deviation of the autocorrelation curve for a specific radius indicate, that we observe a dominant direction of wavefield propagation. We regard therefore the input for the inversion procedure as a robust and unbiased dispersion curve estimate of the fundamental mode.

The inversion results show that we can resolve the uppermost 200m of the structure. We can confirm the shear velocity profile used as a generic model for the German earthquake code (Brüsterle and Stange [29], Brüsterle et al. [30]) as well as results from a previous study (Scherbaum et al. [13]). The shallowest part of the structure can not be determined as the dispersion curve data can not be reliably estimated for frequencies above 1.9 Hz due to the spatial aliasing limit. However, the structural information of this shallow part of the structure is important from the geotechnical point of view and to explain observations of spectral amplification from earthquake data (Ohrnberger et al. [17]). We suggest to perform an additional experiment with adapted aperture for the short wavelength ranges to determine the shallow part of the structure.

## ACKNOWLEDGEMENTS

We thank the members of the SESAME group for helpful discussions, comments and suggestions. All maps and figures were generated with the Generic Mapping Tools GMT (Wessel and Smith, 1991). M. Ohrnberger has been financed by EU-Grant No. EVG1-CT-2000-00026 (SESAME). E. Schissle has been funded by IQN Potsdam (DAAD).

## REFERENCES

1. Borchardt R.D. "Effects of local geological conditions in the San Francisco Bay region on ground motions and the intensities of the 1906 earthquake". Bull. Seism. Soc. Am. 1970: 60, 29-61.
2. Hartzell S., Leeds A., Frankel A., and Michael J. "Site response for urban Los Angeles using aftershocks of the Northridge earthquake". Bull. Seism. Soc. Am. 1996: 86(1B), S168-S192.
3. Yamanaka H. "Geophysical explorations of sedimentary structures and their characterization". Irikura K., Kudo K., Okada H., and Sataini T., Editors. The Effects of Surface Geology on Seismic Motion, Rotterdam, Balkema, 15-33, 1998.
4. Bard, P.-Y. "Microtremor measurements: a tool for site effect estimation?", State-of-the-art paper, Irikura K., Kudo K., Okada H., and Sataini T., Editors. Effects of Surface Geology on Seismic Motion, Yokohama, Rotterdam, Balkema, 3, 1251-1279, 1998.

5. Ishida H., Nozawa T. and Niwa M. "Estimation of deep surface structure based on phase velocities and spectral ratios of long-period microtremors". Irikura K., Kudo K., Okada H., and Satafumi T., Editors. *Effects of Surface Geology on Seismic Motion*, Yokohama, Rotterdam, Balkema, 697–704, 1998.
6. Fäh D., Kind F. and Giardini D. "A theoretical investigation of average H/V ratios", *Geophys. J. Int.* 2001: 145, 535-549.
7. Fäh D., F. Kind and D. Giardini, "Inversion of local S-wave velocity structures from average H/V ratios, and their use for the estimation of site effects". *Journal of Seismology* 2003: 7(4), 449-467.
8. Arai H. and Tokimatsu K. "S-Wave Velocity Profiling by Inversion of Microtremor H/V Spectrum". *Bulletin of the Seismological Society of America* 2004: 94(1), 53–63
9. Horike M. "Inversion of phase velocity of long-period microtremors to the S-wave-velocity structure down to the basement in urbanized area". *J. Phys. Earth* 1985: 33, 59-96.
10. Matsushima T. and Okada H. "Determination of deep geological structures under urban areas using long-period microtremors". *BUTSURI-TANSA* 1990: 43(1), 21-33.
11. Tokimatsu, K., K. Shinzawa, and S. Kuwayama (1992b). "Use of shortperiod microtremors for VS profiling". *J. Geotech. Eng.* 1992: 118(10), 1544–1588.
12. Tokimatsu K. "Geotechnical site characterization using surface waves". Ishihara, Editor. *Earthquake Geotechnical Engineering*, Rotterdam, Balkema 1997: 1333-1368.
13. Scherbaum F., Hinzen K.-G., and Ohrnberger M. "Determination of shallow shear wave velocity profiles in the Cologne, Germany area using ambient vibrations". *Geophys. J. Int.* 2003: 152, 597-612.
14. Forbriger T. "Inversion of shallow-seismic wavefields: II. Inferring subsurface properties from wavefield transforms". *Geophys. J. Int.* 2003: 153, 735–752.
15. Wills C.J. "Differences in Shear-Wave Velocity due to Measurement Methods: A Cautionary Note". *Seism. Res. Lett.* 1998: 69(3), 217-221.
16. Boore D.M. and Brown L.T. "Comparing shear-wave velocity profiles from inversion of surface-wave phase velocities with downhole measurements: systematic differences between CXW method and downhole measurements at six USC strong-motion sites". *Seismol. Res. Lett.* 1998: 69(3), 222-229.
17. Ohrnberger M., Scherbaum F. Krüger F., Pelzing R., Reamer S-K. "How good are shear wave velocity models in the Lower Rhine Embayment (NW-Germany) obtained from inversion of ambient vibrations?" *Bolletino di Geofisica Teorica ed Applicata* 2004, accepted for publication.
18. Bard P.-Y. "The SESAME project: an overview and main results". 13th world conference in Earthquake Engineering, Vancouver, August 2004
19. Atakan K., A.-M. Duval, N. Theodulidis, B. Guillier, J.-L. Chatelain, P.-Y. Bard and SESAME-Team. "The H/V spectral ratio technique: experimental conditions, data processing and empirical reliability assessment". 13th world conference in Earthquake Engineering, Vancouver, August 2004.
20. Duval A.-M., J.-L. Chatelain, B. Guillier and SESAME Project WP02 Team. "Influence of experimental conditions on H/V determination using ambient vibrations (noise)". 13th World Conference on Earthquake Engineering, Vancouver, August 2004.
21. Bonnefoy-Claudet S., Cornou C., Kristek J., Ohrnberger M., Wathelet M., Bard P.-Y., Fäh D., Moczo P., Cotton F., "Simulation of seismic ambient vibrations: I. H/V and array techniques on canonical models". 13th world conference in Earthquake Engineering, Vancouver, August 2004.
22. Cornou C., Kristek J., Bonnefoy-Claudet S., Fäh D., Bard P.-Y., Moczo P., Ohrnberger M., Wathelet M. "Simulation of seismic ambient vibrations: II. H/V and array techniques for real sites". 13th world conference in Earthquake Engineering, Vancouver, August 2004.
23. Ohrnberger, M., Cornou C., Schissele E., Bonnefoy-Claudet S., Wathelet M., Savvaidis A., Scherbaum F., Jongmanns D. "Frequency wavenumber and spatial autocorrelation methods



for dispersion curve determination from ambient vibration recordings". 13th World Conference on Earthquake Engineering, Vancouver, August 2004.

24. Koller M., Lacave C. and others. "Practical user guidelines and software for the implementation of the H/V ratio technique : measuring conditions, processing method and results interpretation". 13th World Conference on Earthquake Engineering, Vancouver, August 2004.

25. Budny M. „Seismische Bestimmung der bodendynamischen Kennwerte von oberflächennahen Schichten in Erdbebengebieten der Niederrheinischen Bucht und ihre ingenieurseismologische Anwendung“. Ph.D. Thesis (in German), Special publications No. 57, Geologisches Institut der Universität zu Köln, pp. 209, 1984.

26. Ibs von Seht M. and Wohlenberg R.; "Microtremor measurements used to map thickness of soft soil sediments". Bull. Seism. Soc. Am. 1999: 89, 250-259.

27. Parolai S., Bormann P. and Milkereit C. "New relationships between vs, thickness of sediments, and resonance frequency calculated by the H/V ratio of seismic noise for Cologne Area (Germany)". Bull. Seism. Soc. Am. 2002: 92, 2521-2527.

28. Hinzen, K.-G., Scherbaum F. and Weber B. "On the resolution of H/V measurements to determine sediment thickness, a case study across a normal fault in the Lower Rhine Embayment, Germany". submitted to JEE, 2003.

29. Brüstle, W. and Stange, S., "Geologische Untergrundklassen zum Entwurf von Normspektren für DIN4149 (neu)", LRGB Baden-Württemberg, AZ: 3480.01/98-4764, 1999.

30. Brüstle, W., Geyer, M., Schmücking, B. „Karte der geologischen Untergrundklassen für DIN 4149 (neu)“. Abschlussbericht, Fraunhofer IRB Verlag, Stuttgart, Best.Nr. T2926, ISBN 3-8167-5766-9, 60 p.

31. Hermann R.B. "Computer programs in seismology, Version 3.0", 1996.

32. Kvaerna T. and Ringdahl F. "Stability of various f-k estimation techniques". Semmiannual technical summary, 1 October 1985 – 31 March 1986, NORSAR Scientific Report, 1-86/87, Kjeller, Norway, 29-40, 1986.

33. Capon J. "High-resolution frequency-wavenumber spectrum analysis". Proc. IEEE 1969: 57, 1408-1418.

34. Brown L.T., Boore D.M., and Stokoe II K.H. "Comparison of Shear-Wave Profiles at 10 Strong-Motion Sites from Noninvasive SASW Measurements and Measurements Made in Boreholes". Bull. Seism. Soc. Am., 2002: 92(8), 3116-3133.

35. Aki K. "Space and time spectra of stationary stochastic waves, with special reference to microtremors", Bull. Earthquake Res. Inst. Tokyo Univ. 1957: 35, 415-456.

36. Bettig B., Bard P.-Y., Scherbaum F., Riepl J., and Cotton F. "Analysis of dense array noise measurements using the modified spatial auto-correlation method (SPAC). Application to the Grenoble area". Bolletino di Geofisica Teorica ed Applicata 2003: 42(3/4), 281-304.

37. Henstridge J.D. "A signal processing method for circular array". Geophysics 1979: 44, 179-184.

38. Sambridge, M. "Geophysical inversion with a neighbourhood algorithm –I. Searching a parameter space". Geophys. J. Int.. 1999: 138, 479-494

39. Sambridge, M. "Geophysical inversion with a neighbourhood algorithm – II. Appraising the ensemble". Geophys. J. Int. 1999: 138, 727-746

40. Wathelet M., Jongmans D. and Ohrnberger M. "Surface wave inversion using a direct search algorithm and its application to ambient vibration measurements". submitted to Near Surface Geophysics, 2003.